Single-shot molecular orbital tomography with orthogonal two-color fields

CHUNYANG ZHAI,[1] XIAOFAN ZHANG,[1] XIAOSONG ZHU,[1,3] LIXIN HE,[1] YINFU ZHANG,[1] BAONING WANG,[1] QINGBIN ZHANG,[1] PENGFEI LAN,[1,*] AND PEIXIANG LU[1,2,4]

[1]*Wuhan National Laboratory for Optoelectronics and School of Physics, Huazhong University of Science and Technology, Wuhan 430074, China*
[2]*Laboratory of Optical Information Technology, Wuhan Institute of Technology, Wuhan 430205, China*
[3]*zhuxiaosong@hust.edu.cn*
[4]*lupeixiang@hust.edu.cn*
[*]*pengfeilan@hust.edu.cn*

Abstract: Molecular orbital tomography (MOT) based on high-order-harmonic generation opens a way to track the molecular electron dynamics or even follow a chemical reaction. However, the real-time imaging of the evolution of electron orbitals is hampered by the multi-shot measurement of high-order harmonics. Here, we report a single-shot MOT scheme with orthogonal two-color (OTC) fields. This scheme enables the tomographic imaging of molecular orbital with single-shot measurement in experiment, owing to the two-dimensional manipulation of the electron motion in OTC fields. Our work paves the way towards tracking the molecular electron dynamics with combined attosecond temporal and sub-Ångström spatial resolutions.

References and links

1. P. Hockett, C. Z. Bisgaard, O. J. Clarkin, and A. Stolow, "Time-resolved imaging of purely valence-electron dynamics during a chemical reaction," Nat. Phys. **7**, 612–615 (2011).
2. X. Xie, S. Roither, D. Kartashov, E. Persson, D. G. Arbö, L. Zhang, S. Gräfe, M. S. Schöffler, J. Burgdörfer, A. Baltuška, and M. Kitzler, "Attosecond probe of valence-electron wave packets by subcycle sculpted laser fields," Phys. Rev. Lett. **108**, 193004 (2012).
3. B. Barwick and A. H. Zewail, "Photonics and plasmonics in 4D ultrafast electron microscopy," ACS Photon. **2**, 1391–1402 (2015).
4. W. A. Okell, T. Witting, D. Fabris, C. A. Arrell, J. Hengster, S. Ibrahimkutty, A. Seiler, M. Barthelmess, S. Stankov, D. Y. Lei, Y. Sonnefraud, M. Rahmani, T. Uphues, S. A. Maier, J. P. Marangos, and J. W. G. Tisch, "Temporal broadening of attosecond photoelectron wavepackets from solid surfaces," Optica **2**, 383–387 (2015).
5. A. S. Wyatt, T. Witting, A. Schiavi, D. Fabris, P. M. Hernando, I. A. Walmsley, J. P. Marangos, and J. W. G. Tisch, "Attosecond sampling of arbitrary optical waveforms," Optica **3**, 303–310 (2016).
6. P. Lan, M. Ruhmann, L. He, C. Zhai, F. Wang, X. Zhu, Q. Zhang, Y. Zhou, M. Li, M. Lein, and P. Lu, "Attosecond probing of nuclear dynamics with trajectory-resolved high-harmonic spectroscopy," Phys. Rev. Lett. **119**, 033201 (2017).
7. C. I. Blaga, J. Xu, A. D. DiChiara, E. Sistrunk, K. Zhang, P. Agostini, T. A. Miller, L. F. DiMauro, and C. D. Lin, "Imaging ultrafast molecular dynamics with laser-induced electron diffraction," Nature **483**, 194–197 (2012).
8. H. Niikura, F. Légaré, R. Hasbani, A. D. Bandrauk, M. Ivanov, D. M. Villeneuve, and P. B. Corkum, "Sub-laser-cycle electron pulses for probing molecular dynamics," Nature **417**, 917–922 (2002).
9. W. Li, X. Zhou, R. Lock, S. Patchkovskii, A. Stolow, H. C. Kapteyn, and M. M. Murnane, "Time-resolved dynamics in N_2O_4 probed using high harmonic generation," Science **322**, 1207–1211 (2008).
10. P. W. Hawkes and J. C. H. Spence, eds., *Science of Microscopy*, (Springer, 2007).
11. M. Th. Hassan, J. S. Baskin, B. Liao, and A. H. Zewail, "High-temporal-resolution electron microscopy for imaging ultrafast electron dynamics," Nat. Photon. **11**, 425–430 (2017).
12. B. Wolter, M. G. Pullen, A.-T. Le, M. Baudisch, K. Doblhoff-Dier, A. Senftleben, M. Hemmer, C. D. Schröter, J. Ullrich, T. Pfeifer, R. Moshammer, S. Gräfe, O. Vendrell, C. D. Lin, and J. Biegert, "Ultrafast electron diffraction imaging of bond breaking in di-ionized acetylene," Science **354**, 308–312 (2016).

13. J. Miao, P. Charalambous, J. Kirz, and D. Sayre, "Extending the methodology of X-ray crystallography to allow imaging of micrometre-sized non-crystalline specimens," Nature **400**, 342–344 (1999).
14. Y. Huismans, A. Rouzée, A. Gijsbertsen, J. H. Jungmann, A. S. Smolkowska, P. S. W. M. Logman, F. Lépine, C. Cauchy, S. Zamith, T. Marchenko, J. M. Bakker, G. Berden, B. Redlich, A. F. G. van der Meer, H. G. Muller, W. Vermin, K. J. Schafer, M. Spanner, M. Yu. Ivanov, O. Smirnova, D. Bauer, S. V. Popruzhenko, and M. J. J. Vrakking, "Time-resolved holography with photoelectrons," Science **331**, 61–64 (2011).
15. J. M. Glownia, A. Natan, J. P. Cryan, R. Hartsock, M. Kozina, M. P. Minitti, S. Nelson, J. Robinson, T. Sato, T. van Driel, G. Welch, C. Weninger, D. Zhu, and P. H. Bucksbaum, "Self-referenced coherent diffraction X-ray movie of Ångström- and femtosecond-scale atomic motion," Phys. Rev. Lett. **117**, 153003 (2016).
16. T. Elsaesser and M. Woerner, "Photoinduced structural dynamics of polar solids studied by femtosecond X-ray diffraction," Acta Crystallogr A **66**, 168–178 (2010).
17. M. Gao, C. Lu, H. Jean-Ruel, L. C. Liu, A. Marx, K. Onda, S. Y. Koshihara, Y. Nakano, X. Shao, T. Hiramatsu, G. Saito, H. Yamochi, R. R. Cooney, G. Moriena, G. Sciaini, and R. J. Miller, "Mapping molecular motions leading to charge delocalization with ultrabright electrons," Nature **496**, 343–346 (2013).
18. M. Meckel, D. Comtois, D. Zeidler, A. Staudte, D. Pavičić, H. C. Bandulet, H. Pépin, J. C. Kieffer, R. Dörner, D. M. Villeneuve and P. B. Corkum, "Laser-induced electron tunneling and diffraction," Science **320**, 1478–1482 (2008).
19. R. Srinivasan, J. S. Feenstra, S. T. Park, S. Xu, and A. H. Zewail, "Dark structures in molecular radiationless transitions determined by ultrafast diffraction," Science **307**, 558–563 (2005).
20. J. Itatani, J. Levesque, D. Zeidler, H. Niikura, H. Pépin, J. C. Kieffer, P. B. Corkum, and D. M. Villeneuve, "Tomographic imaging of molecular orbitals," Nature **432**, 867–871 (2004).
21. S. Haessler, J. Caillat, and P. Salières, "Self-probing of molecules with high harmonic generation," J. Phys. B: At. Mol. Opt. Phys. **44**, 203001(2011).
22. P. B. Corkum, "Plasma perspective on strong-field multiphoton ionization," Phys. Rev. Lett. **71**, 1994 (1993).
23. P. Salières, A. Maquet, S. Haessler, J. Caillat, and R. Taïeb, "Imaging orbitals with attosecond and Ångström resolutions: toward attochemistry?" Rep. Prog. Phys. **75**, 062401 (2012).
24. C. Vozzi, M. Negro, F. Calegari, G. Sansone, M. Nisoli, S. De Silvestri, and S. Stagira, "Generalized molecular orbital tomography," Nat. Phys. **7**, 822–826 (2011).
25. J. B. Bertrand, H. J. Wörner, P. Salières, D. M. Villeneuve, and P. B. Corkum, "Linked attosecond phase interferometry for molecular frame measurements," Nat. Phys. **9**, 174–178 (2013).
26. C. Zhai, X. Zhu, P. Lan, F. Wang, L. He, W. Shi, Y. Li, M. Li, Q. Zhang, and P. Lu, "Diffractive molecular-orbital tomography," Phys. Rev. A **95**, 033420 (2017).
27. S. Haessler, J. Caillat, W. Boutu, C. Giovanetti-Teixeira, T. Ruchon, T. Auguste, Z. Diveki, P. Breger, A. Maquet, B. Carré, R. Taïeb, and P. Salières, "Attosecond imaging of molecular electronic wavepackets," Nat. Phys. **6**, 200–206 (2010).
28. H. Stapelfeldt and T. Seideman, "Colloquium: Aligning molecules with strong laser pulses," Rev. Mod. Phys. **75**,543–557 (2003).
29. D. Shafir, Y. Mairesse, D. M. Villeneuve, P. B. Corkum, and N. Dudovich, "Atomic wavefunctions probed through strong-field light–matter interaction," Nat. Phys. **5**, 412–416 (2009).
30. H. Niikura, N. Dudovich, D. M. Villeneuve, and P. B. Corkum, "Mapping molecular orbital symmetry on high-order harmonic generation spectrum using two-color laser fields," Phys. Rev. Lett. **105**, 053003 (2010).
31. M. Kitzler, X. Xie, A. Scrinzi, and A. Baltuska, "Optical attosecond mapping by polarization selective detection," Phys. Rev. A **76**, 011801 (2007).
32. X. M. Tong, Z. X. Zhao, and C. D. Lin, "Theory of molecular tunneling ionization," Phys. Rev. A **66**, 033402 (2002).
33. D. Pavičić, K. F. Lee, D. M. Rayner, P. B. Corkum, and D. M. Villeneuve, "Direct measurement of the angular dependence of ionization for N_2, O_2, and CO_2 in intense laser fields," Phys. Rev. Lett. **98**, 243001 (2007).
34. K. Yoshii, G. Miyaji, and K. Miyazaki, "Retrieving angular distributions of high-order harmonic generation from a single molecule," Phys. Rev. Lett. **106**, 013904 (2011).
35. B. K. McFarland, J. P. Farrell, P. H. Bucksbaum, and M. Gühr, "High harmonic generation from multiple orbitals in N_2," Science **322**, 1232–1235 (2008).
36. D. Shafir, H. Soifer, B. D. Bruner, M. Dagan, Y. Mairesse, S. Patchkovskii, M. Yu. Ivanov, O. Smirnova, and N. Dudovich, "Resolving the time when an electron exits a tunnelling barrier," Nature **485**, 343–346 (2012).
37. S. Luo, M. Li, H. Xie, P. Zhang, S. Xu, Y. Li, Y. Zhou, P. Lan, and P. Lu, "Angular-dependent asymmetries of above-threshold ionization in a two-color laser field," Phys. Rev. A **96**, 023417 (2017).
38. K. J. Yuan and A. D. Bandrauk, "Single circularly polarized attosecond pulse generation by intense few cycle elliptically polarized laser pulses and terahertz fields from molecular media," Phys. Rev. Lett. **110**, 023003 (2013).
39. N. B. Delone and V. P. Krainov, "Energy and angular electron spectra for the tunnel ionization of atoms by strong low-frequency radiation," J. Opt. Soc. Am. B **8**, 1207–1211 (1991).
40. H. Yun, K. Lee, J. H. Sung, K. T. Kim, H. T. Kim, and C. H. Nam, "Resolving multiple molecular orbitals using two-dimensional high-harmonic spectroscopy," Phys. Rev. Lett. **114**, 153901 (2015).
41. I. J. Kim, C. M. Kim, H. T. Kim, G. H. Lee, Y. S. Lee, J. Y. Park, D. J. Cho, and C. H. Nam, "Highly efficient high-harmonic generation in an orthogonally polarized two-color laser field," Phys. Rev. Lett. **94**, 243901 (2005).
42. M. Lewenstein, P. Balcou, M. Y. Ivanov, A. L'Huillier, and P. B. Corkum, "Theory of high-harmonic generation by low-frequency laser fields," Phys. Rev. A **49**, 2117 (1994).

43. B. Shan, S. Ghimire, and Z. Chang, "Effect of orbital symmetry on high-order harmonic generation from molecules," Phys. Rev. A **69**, 021404 (2004).
44. M. J. Frisch, G. W. Trucks, H. B. Schlegel, G. E. Scuseria, M. A. Robb, J. R. Cheeseman, G. Scalmani, V. Barone, B. Mennucci, G. A. Petersson, H. Nakatsuji, M. Caricato, X. Li, H. P. Hratchian, A. F. Izmaylov, J. Bloino, G. Zheng, J. L. Sonnenberg, M. Hada, M. Ehara, K. Toyota, R. Fukuda, J. Hasegawa, M. Ishida, T. Nakajima, Y. Honda, O. Kitao, H. Nakai, T. Vreven, J. A. Montgomery, Jr., J. E. Peralta, F. Ogliaro, M. Bearpark, J. J. Heyd, E. Brothers, K. N. Kudin, V. N. Staroverov, R. Kobayashi, J. Normand, K. Raghavachari, A. Rendell, J. C. Burant, S. S. Iyengar, J. Tomasi, M. Cossi, N. Rega, J. M. Millam, M. Klene, J. E. Knox, J. B. Cross, V. Bakken, C. Adamo, J. Jaramillo, R. Gomperts, R. E. Stratmann, O. Yazyev, A. J. Austin, R. Cammi, C. Pomelli, J. W. Ochterski, R. L. Martin, K. Morokuma, V. G. Zakrzewski, G. A. Voth, P. Salvador, J. J. Dannenberg, S. Dapprich, A. D. Daniels, Ö. Farkas, J. B. Foresman, J. V. Ortiz, J. Cioslowski, and D. J. Fox, Gaussian 09, Revision D.01. Gaussian, Inc., Wallingford CT, (2009).
45. S. A. Rezvani, Z. Hong, X. Pang, S. Wu, Q. Zhang, and P. Lu, "Ultrabroadband tunable OPA design using a spectrally broadened pump source," Opt. Lett. **42**, 3367–3370 (2017).

1. Introduction

Real-time tracking of molecular electron dynamics with high spatial and temporal resolutions is the dream of ultrafast scientists [1–9]. In the past decades, a variety of imaging techniques, either based on lens, e.g., optical or electron microscopy [10–12], or lensless, e.g., coherent diffractive imaging (CDI) [13] and holography [14], have been developed. The advancements of these imaging techniques have expanded our knowledge about the static structures of matter. Nanometer scale or even better resolution has been obtained with ultrashort x-ray beams [15, 16] and electron beams [17–19]. However, the temporal resolution is limited to several tens or several hundreds femtoseconds at present.

To get the real-time evolution of the molecular electron dynamics, i.e., a molecular movie, one need to make the measurement of the ultrafast processes a reality with unprecedented attosecond and sub-Ångström resolutions. In recent years, an alternative way, called molecular orbital tomography (MOT) [20, 21], is developed. It is based on high-order-harmonic generation (HHG) that results from the interaction of femtosecond lasers with atoms and molecules. The information of the target molecular structure and dynamics is encoded in the high-order-harmonic spectra. According to the three-step recollision model of HHG [22], the spatial resolution for the structures is determined by the de Broglie wavelength of the returning electrons, which is typically in the Ångström scale [23]. Besides, the HHG signal intrinsically has the subfemtosecond resolution, because the HHG is produced by the electron recollision in a subcycle of the laser field. Therefore, the most important aspect of MOT based on the HHG is that it holds the potential to make the molecular movies.

However, there are several roadblocks when capturing the snapshot of molecular orbitals at present. One roadblock is the measurement of harmonic phase requires sophisticated techniques and represents formidable challenges at present [24, 25]. By exploiting CDI technique in conjunction with MOT method [26], it was shown that the problem of phase measurement can be overcome. The other roadblock is that MOT requires the measurement of high-order harmonics as a function of both the harmonic order and the recombination angle [20, 27]. One needs to align molecules and measure the high-order-harmonic spectra by scanning the alignment angles. Although laser-assisted molecular alignment has become a mature tool [28], the measurement of the high-order harmonics generated at a series of alignment angles requires multi-shot experiments. To effectively capture the snapshot of molecular orbitals, single-shot experiment is desired.

In this paper, we report a new scheme for single-shot MOT with orthogonal two-color (OTC) fields. By controlling the two-dimensional trajectory of the electron with the OTC fields, the electron can recombine with the parent ion from different angles, which enables us to probe the target molecules with only single-shot measurement. In the proof-of-principle experiment, the molecular orbital of N_2 has been reconstructed by solely measuring the intensity of HHG with

OTC fields.

2. Principle of the scheme

To explain the single-shot MOT scheme, we briefly outline the method of MOT. Based on the original MOT theory [20], in the recombination step of the HHG process, the returning continuum electron wave packets are approximated as plane waves and the recombination dipole moment **d** in the velocity form reads

$$\mathbf{d}(\mathbf{k}, \varphi_k) = \mathbf{k}\langle\Psi|\mathbf{k}\rangle = \mathbf{k}\mathcal{F}[\Psi], \tag{1}$$

where **k** and φ_k are the momentum and recombination angle relative to the molecule of the returning electron, respectively. Ψ is the molecular orbital. One can see that Ψ and $\mathbf{d}(\mathbf{k},\varphi_k)/\mathbf{k}$ is a Fourier transform pair. $\mathbf{d}(\mathbf{k},\varphi_k)$ and $\mathbf{d}(\mathbf{k},\varphi_k)/\mathbf{k}$ can be obtained from the experimental measurement of HHG spectra. Then we can reconstruct the orbital Ψ by inverse Fourier transform of the measured $\mathbf{d}(\mathbf{k},\varphi_k)/\mathbf{k}$. For this scheme, it is required to measure the spectral map as a function of the harmonic order and the recombination angle. In a linearly polarized laser field, the returning electron is driven back only along the laser polarization direction. Therefore, to reconstruct the orbital Ψ, one has to align the molecule and measure the HHG spectra for all the different alignment angles, i.e. the multi-shot measurement is required.

To overcome the requirement of multi-shot measurement, in this work, we use an OTC field to control the two-dimensional trajectory of the electron [29–31]. As a result, different recombination angles can map to different harmonic orders in the molecular frame. Then, we can obtain the information at different recombination angles with single-shot measurement. To explain the principle of our scheme, we take the example of N_2 to demonstrate the effective control of the electron two-dimensional trajectory with OTC fields. According to the molecular Ammosov-Delone-Krainov (MO-ADK) theory [32], N_2 molecule is mainly ionized at the direction parallel to the molecular axis. Therefore, for randomly aligned N_2 molecules, the molecules parallel to the instantaneous direction of the synthesized electric field combined by the two color laser
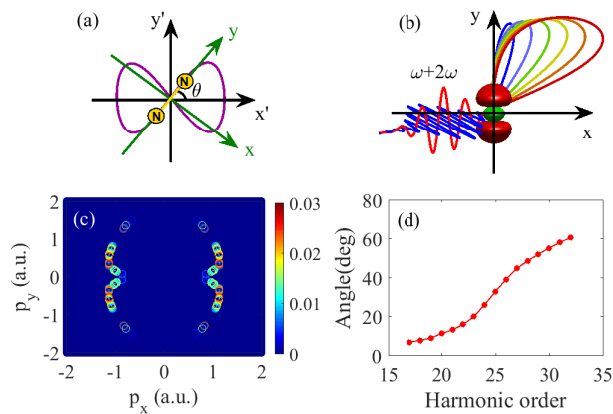

Fig. 1. (a), Illustration the laboratory frame (x′, y′) and the molecular frame (x, y). The purple line shows the Lissajous diagram of the OTC field read in the laboratory frame.The molecular frame rotates with the instantaneous electric field direction. (b), Schematic drawings of the electronic trajectories in the molecular frame driven by the OTC field. (c), The momentum distribution of the returning electron obtained from the semiclassical calculation. One can see that it presents an 8-like shape relative to the molecular frame. (d), Calculated recombination angles of different harmonic orders for N_2 in the molecular frame.

fields are preferentially ionized [33]. Then, HHG is also dominantly contributed by the molecules parallel to the instantaneous electric field direction [34]. In this case, the HHG are expected to be dominant by the contribution of the highest occupied molecular orbital (HOMO). This also allows us to minimize the multiple orbitals effect on HHG [30, 35].

For clarity, we define two different reference frames. One is the laboratory frame (x′, y′), in which the x′ axis is parallel to the fundamental component and the y′ axis is parallel to the second harmonic (SH) component of the OTC field, respectively [see Fig. 1(a)]. The other one is the molecular frame (x, y). As shown in Figs. 1(a) and 1(b) for N_2, the y axis is parallel to the molecular axis (parallel to the instantaneous maximum field direction in which the electron is ionized). Note that, as in [36], different order harmonics are contributed by electrons with different ionization times and recombination times. Consequently, different harmonics correspond to different recombination directions in either the laboratory frame or the molecular frame. The electron trajectories in the molecular frame are illustrated in Fig. 1(b). In contrast to linearly polarized laser field, one can see that the OTC field can effectively control the electron two-dimensional trajectory [29]. The returning electrons with different momenta are driven to recombine with the parent ion at different angles relative to the molecule. To characterize the returning electron, we calculate the electron trajectories in the molecular frame in the synthesized electric field. The synthesized OTC field consists of the fundamental 800-nm and its SH 400-nm components in orthogonal polarizations. The durations (full width at half-maximum) and intensities of both the 800-nm field and the 400-nm field are 30-fs and 1.8×10^{14} W/cm^2. The OTC electric field is given by [atomic units (a.u.) $e = \hbar = m_e = 1$ are used, unless otherwise noted]

$$\vec{E}(t) = E_{x'} f_{x'}(t)\cos(\omega t)\vec{e}_{x'} + E_{y'} f_{y'}(t)\cos(2\omega t + \phi)\vec{e}_{y'}, \qquad (2)$$

where $E_{x'}$, $E_{y'}$ and ω, 2ω are the amplitudes and frequencies of the fundamental and the SH fields, respectively. ϕ is the relative phase between the two fields, which can be adjusted by a pair of wedges in experiment [37]. The envelopes $f_{x'}(t)$ and $f_{y'}(t)$ of the pulses are Gaussian. According to [22], the electron trajectory is calculated with the classical model [38]. Because a multi-cycle OTC pulse is used, we only consider the electron trajectories within one optical cycle of the fundamental pulse. Every classical return receives a weight $W(t_0, v_\perp)$ based on the tunnelling probability [38]. The weight is calculated by

$$W(t_0, v_\perp) = W_0(t_0)W_1(v_\perp), \qquad (3)$$

where $W_0(t_0)$ is the ionization rate at time t_0 and $W_1(v_\perp)$ is the weight with a Gaussian distribution for the tunnel electron with initial transverse velocity $v_\perp$ [39]. Further details of the calculations are described in the Appendix.

The returning electron momentum distribution in the molecular frame with relative phase $\phi=0.5\pi$ is shown in Fig. 1(c). The colorbar reflects the weight of return probability. Figure 1 (c) presents an 8-like shape distribution, i.e., the electrons with different momenta recombine with the parent ion at different angles. From Fig. 1(c), we can calculate the recombination angles φ_k as a function of the harmonic order (see the Appendix). The results are shown in Fig. 1(d). Note that, due to the symmetry of the distribution, only the results in the first quadrant are plotted. It is evident from Fig. 1(d) that, there is a one-to-one map between the harmonic order and the recombination angle of the returning electron. In contrast, all the harmonics map to one recombination angle in the linearly polarized field. Herein, the recombination angle covers almost the whole range from 0° to 360°. This makes it possible to retrieve the molecular orbital with single-shot experiment. It should be noted that the spectral range in our experiment is limited from 17*th* to 32*nd* harmonics. Therefore, we calculate the same spectral range in Figs. 1(c) and 1(d). By increasing the laser intensity or the wavelength of the OTC field, we can increase the spectral range. The one-to-one map between the harmonic order and the recombination angle still holds.
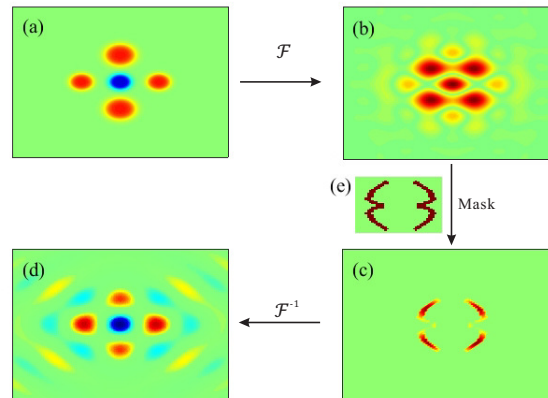
Fig. 2. (a), A model "sample" in coordinate space. (b), The Fourier transform spectrum of the model "sample". (c), The Fourier transform spectrum of the model "sample" is multiplied by an 8-like mask. (d), The model "sample" is reconstructed by inverse Fourier transforming of the partial spectrum shown in Fig. 2(c). (e), The shape of the mask M.

As shown in Figs. 1(c) and 1(d), although the returning electron momentum distribution covers almost all the directions from $0°$ to $360°$ in the OTC field, there is only one harmonic order mapping to one recombination angle. In other words, in the Fourier space (p_x, p_y), only limited information of the N_2 molecular orbital is sampled. Is such sparse information sufficient to reconstruct the molecular orbital? This problem can be recasted to a more general question: can we retrieve the structure of an unknown function $f(r)$ from a partial of its Fourier transform $\mathcal{F}[f(r)]$. To address this problem, a proof of the principle simulation is illustrated in Fig. 2. Figure 2(a) shows the model "sample", i.e., $f(r)$, in coordinate space. Figure 2(b) is the Fourier transform spectrum of the sample in the Fourier space, i.e., $\mathcal{F}[f(r)]$. In order to mimic the sampling in Fig. 1(c), an 8-like mask function M [see Fig. 2(e)] with the same distribution as in Fig. 1(c) is multiplied to $\mathcal{F}[f(r)]$. The partial spectrum of the Fourier transform $M\mathcal{F}[f(r)]$ is shown in Fig. 2(c). By inverse Fourier transforming the partial spectrum, one obtains the reconstructed sample in coordinate space shown in Fig. 2(d). Note that because only limited information filtered by the mask is sampled, one can see extra oscillation and some minor distortion of the main lobes compared with the target sample. However, one can see that the reconstructed sample reproduces the main features of the target sample: it contains one negative and four positive lobes and the positions of the lobes are the same as those in the target sample. This result indicates that partial sampling is sufficient to reconstruct the main structure of the target sample. It is worth noting that the diffraction spectrogram is always partially sampled in the well-known x-ray CDI and holography experiment. It is because the low frequency components are usually blocked and the high frequency components are very weak and cannot be measured due to the limitation of the dynamic range of the detector. However, it does not prevent from imaging the target sample although some fine structure information can be lost and the spatial resolution gets worse.

3. Experiment and results

To demonstrate the single-shot MOT scheme, we perform the experiment by using a commercial Ti:sapphire laser system (Legend Elite-Duo, Coherent, Inc.). It delivers a 30-fs, 800-nm pulse with the maximum energy of 10 mJ per shot at a repetition rate of 1 kHz. Figure 3 shows a schematic layout of the experiment. For the SH generation, a beta-barium borate (β-BBO) crystal (300 μm thick, type I) is used. A dual waveplate (DW1) and a wire grid polarizer (WGP) are used
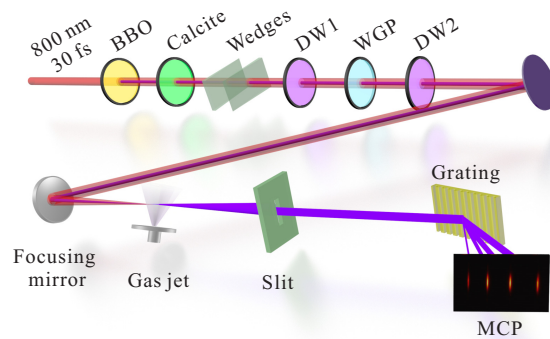
Fig. 3. Schematic of the experimental setup. A second harmonic is produced using a type-I BBO crystal rotated away from the optimum phase-matching angle. The SH field is orthogonally polarized with respect to the fundamental field. Group-velocity dispersion is compensated using a calcite plate. The relative phase of the SH field relative to the fundamental field is controlled with a pair of wedges. DW1 and DW2 are dual waveplates ($\lambda/2$ at 800 nm and λ at 400 nm). WGP is a wire grid polarizer. DW1 and WGP are used to adjust the fundamental field energy. DW2 is used to adjust the polarization state of fundamental field to orthogonally polarized with respect to the SH field. High-order harmonics are generated by focusing the two beams with a spherical mirror onto a gas jet. The harmonic spectrum is measured by an extreme-ultraviolet spectrometer.

to continuously control the fundamental field energy. The dual waveplate is a half-wave plate for the fundamental pulse and a full-wave plate for the SH pulse. Then the polarization of the fundamental field is rotated to be orthogonal polarization with the SH field using another dual waveplate (DW2). The time delay and the relative phase between the fundamental and the SH fields are adjusted using a calcite plate (1.4 mm thick) and a pair of wedges (2.8° wedge angle), respectively. By stepping one of the wedges with a motorized Gothic-Arch Bearing stage, the relative phase between the fundamental and the SH fields is fine controlled. The relative phase between the fundamental and SH fields is measured by observing the HHG yield as a function of relative phase. According to [40, 41], the relative phase of the OTC fields is identified to be 0.5π when the even harmonic yield from argon gas is maximized. The OTC fields are focused onto a supersonic gas jet by a spherical mirror (f=300 mm). In our experiment, by adjusting both DW1
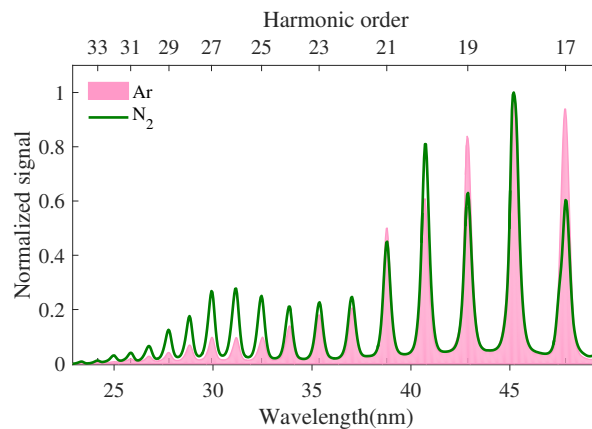

Fig. 4. High-order-harmonic spectra measured in N_2 (green line) and argon (full-filled) with OTC fields.

and WGP, we can selectively obtain one component of either the fundamental or the SH field interacting with the gas. Then the laser intensities of the fundamental and the SH fields in the interaction region are estimated by the harmonic cutoff when only one component interact with the gas. The emitted high-order harmonics are dispersed by a slit (0.1 mm wide and 15 mm high) and a flat-field grating (1200 grooves/mm). Then the high-order harmonics are imaged onto the microchannel plate (MCP) fitted with a phosphor screen. The image on the screen is read out by a charge-coupled device (CCD) camera. Figure 4 displays the high-order-harmonic spectra for argon (full-filled) and N_2 (green line).

To obtain the amplitude of the recombination dipole moment of the molecule, the harmonic signal from N_2 molecules is calibrated with that of a reference atom (argon) [20] which has nearly the same ionization potential. The amplitude of the dipole moment of the reference atom $d^{ref}(k)$ is calculated by [20,42,43]

$$d^{ref}(k) = \frac{2^{5/2}}{\pi}(2I_p)^{5/4}\frac{k}{(k^2+2I_p)^2}.$$ (4)

Note that, the velocity form is used in our work. Then the amplitude of the dipole momentum of the molecule is obtained as

$$d(k,\varphi_k) = \sqrt{\frac{A^{mol}(k,\varphi_k)}{A^{ref}(k)}}d^{ref}(k),$$ (5)

where A^{mol} and A^{ref} denote the intensities of the measured high-order harmonics of the molecule and the reference atom, respectively. The recombination angle φ_k can be obtained from Fig. 1(d) for each harmonic order. After the recombination dipole moment of N_2 molecular orbital is extracted, for convenience, we define $D(k,\varphi_k)=d(k,\varphi_k)/k$. Note that only the amplitude is measured in our experiment. To overcome the difficulty of phase measurement, we retrieve the phase and then the molecular orbital with a previously developed iterative algorithm based on the combination of CDI with MOT [26].

With the single-shot MOT scheme, we reconstruct the HOMO of N_2 from the experimental data. The reconstructed HOMO is shown in Fig. 5(a). For comparison, we calculate the exact
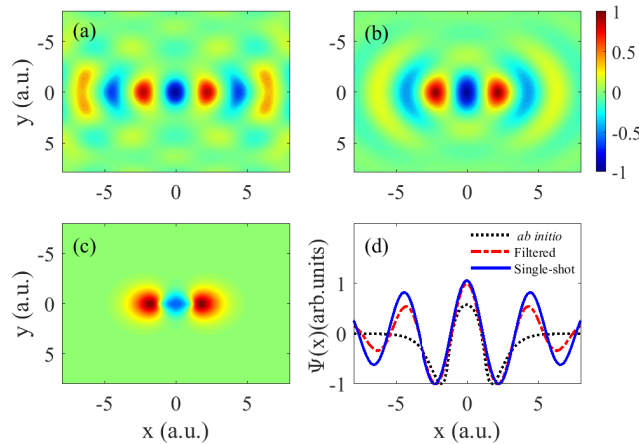

Fig. 5. Reconstructed HOMO of N_2. (a), Reconstructed HOMO from the experimental data. (b), Filtered *ab initio* orbital simulated with the limited spectral range according to the experimental conditions. (c), Calculated *ab initio* orbital with the *ab initio* model. (d), Cuts along the internuclear axis for the molecular orbitals.

HOMO of N_2 with *ab initio* calculation [44] and the result is shown in Fig. 5(c). By comparing Figs. 5(a) and 5(c), our reconstructed HOMO possesses the main characteristics of the exact HOMO of N_2, namely three main lobes with alternating signs, separated by two nodal surfaces. Some additional structures appear away from the center lobs, i.e., for |x|>5 a.u. [see Fig. 5(a)], compared with the *ab initio* orbital [see Fig. 5(c)]. This is owing to the limited spectral range and sparse sampling of HHG in our single-shot MOT scheme. To mimic this effect, we have calculated the restricted recombination dipoles from the *ab initio* orbital over the spectral range according to our experiment. Then, as in Fig. 2, the orbital (which we call the filtered orbital) is obtained by the inverse Fourier transform of the restricted dipoles. The result is shown in Fig. 5(b). The filtered *ab initio* orbital has the similar additional structures and is in good agreement with the experimental reconstruction [see Figs. 5(a) and 5(b)]. This confirms that, the additional structures are mainly due to the limited spectral range applied in the measurement [23, 27]. For clarity, the line profile along the internuclear axis for the experimental reconstruction (blue solid line), the filtered *ab initio* orbital (red dash-dotted line), and the *ab initio* orbital (black dashed line) are presented in Fig. 5(d). The internuclear distance (defined as the distance between the nodes along the molecular axis) obtained from the experimental reconstruction is R=2.19 a.u., which is close to that of the filtered *ab initio* orbital (R=2.13 a.u.) and also agrees well with the *ab initio* orbital (R=2.06 a.u.). The slight difference between the reconstructed result and the *ab initio* orbital is a trade-off between the good resolution and the easy measurement in our single-shot experimental conditions. According to the theory of our proposed single-shot molecular orbital tomography and the above discussions, targets with the following qualifications will be suitable for our method: (1) The object is axially-symmetric. (2) The radial part vanishes outside the range covered by the measurement, i.e., the range of the plateau harmonic is large enough to cover the major distribution of orbital in momentum space. (3) The angular and radial components of the object are factorizable. In order to further optimize the reconstructed results, it is a promising option to apply driving lasers with longer central wavelengths (e.g. the middle-infrared lasers) that can be generated by optical parametric amplifier [45]. The middle-infrared lasers can extend the cutoff of high-order harmonics with a modest intensity for the molecule.

4. Conclusion

In conclusion, we have demonstrated a single-shot MOT scheme for imaging the molecular orbital with OTC fields. It is shown that the electron can recombine with the parent ion from different angles in the OTC field, enabling to probe the molecular orbital with only single-shot measurement. By using the single-shot MOT scheme, the HOMO of N_2 has been well reconstructed. It circumvents the hurdle of multi-shot measurements in experiment, making a substantial step towards the goal of molecular movie.

Appendix

Here we describe the details of the calculation in Section 2.

First, we calculate the ionization probability $W(t_0, v_\perp)$:

$$W(t_0, v_\perp) = W_0(t_0)W_1(v_\perp). \tag{6}$$

$W_0(t_0)$ is the ionization rate at time t_0 and is given by the MO-ADK model [32, 38]. $W_1(v_\perp)$ is the weight for the tunneling electron with initial transverse velocity $v_\perp$ [39]:

$$W_1(v_\perp) = \exp[-\sqrt{2I_p}v_\perp^2/E(t_0)]. \tag{7}$$

Second, the evolution of the electron (ionized at t_0) is described by classical equations in

laboratory frame [38]

$$\ddot{\mathbf{r}}(t) = -\vec{E}(t), \tag{8}$$

$$\dot{\mathbf{r}}_x(t_0) = -v_\perp \sin(\theta_E), \tag{9}$$

$$\dot{\mathbf{r}}_y(t_0) = v_\perp \cos(\theta_E), \tag{10}$$

$$\mathbf{r}(t_0) = 0, \tag{11}$$

where $\mathbf{r}$ is the position vector of the electron. $\vec{E}(t)$ is the OTC field that described in Eq.(2). θ_E is the angle between the direction of the instantaneous electric field at ionization time t_0 and the major ionization direction of the molecule. Taking N_2 as an example, the molecules paralleled to the instantaneous electric field direction are dominantly ionized in randomly aligned molecules [32–34]. Therefore, θ_E is zero for N_2. When the electron approaches the parent ion within a distance of 1 a.u, the recollision occurs. For each recollision, the returning electron is weighted by the ionization probability $W(t_0, v_\perp)$.

Third, when the electron recollides with the core, the returning momenta $k_{x'}$ and $k_{y'}$ in laboratory frame are obtained. Using the returning momenta $k_{x'}$ and $k_{y'}$, the recombination angle α in molecular frame can be obtained

$$\alpha = \arctan(k_x/k_y), \tag{12}$$

where $k_x = k_{x'}\cos(\theta) + k_{y'}\sin(\theta)$ and $k_y = -k_{x'}\sin(\theta) + k_{y'}\cos(\theta)$ are the returning momenta in molecular frame as shown in Fig. 1(c). θ is the instantaneous angle between the x-axis of the molecular frame and the x' axis of the laboratory frame, and it is calculated as $\theta = \arctan(E_{x'}(t_0)/E_{y'}(t_0))$. The kinetic energy of the electron at returning time is $E_k = (k_x^2 + k_y^2)/2$. This is associated with the harmonic photon energy, $q\omega$, via energy conservation: $q\hbar\omega = E_k + I_p$, where ω is the frequency of fundamental laser field and q is the harmonic order. I_p is the ionization potential. Figure 1(d) shows the relation between the harmonic order and the recombination angle in the first quadrant. It is found that the harmonic order and the recombination angle are one-to-one correspondence, which gives the chance to identify the different recombination angles through different harmonic orders.